Int. J. Heat Mass Transfer. Vol. 16. pp. 2393–2406. Pergamon Press 1973. Printed in Great Britain

NUMERICAL APPROACH TO NON-SPHERICAL VAPOUR BUBBLE DYNAMICS

T. B. GUY and T. J. LEDWIDGE
Engineering Research Division
Australian Atomic Energy Commission Research Establishment, Lucas Heights

(*Received* 27 *February* 1973 *and in revised form* 1 *June* 1973)

Abstract—An explicit finite difference analysis has been applied to the growth and collapse of a vapour bubble in sub-cooled water. It is assumed that only mass transfer across the liquid–vapour interface is important and that heat transfer can be neglected. The results of this computational analysis are compared with experimental results from the literature and shown to be in good agreement at sub-cooling of 1 C and 10 C.

For these experimental conditions the analysis shows that the bubble grows in a roughly spherical fashion but collapses in highly non-spherical manner.

NOMENCLATURE

a, diameter of nucleation site hole;
a_f, thickness of the annular region occupied by the liquid at the base of the bubble;
A, elemental bubble surface area;
A_b, area of liquid film at base of bubble;
A_s, surface area of the liquid film at the base of the bubble;
B, constant equation (15) ($B = 4{\cdot}89 \times 10^3$ when ρ^* lb/in^3 and T_LK° used);
C, constant equation (10);
C_L, heat capacity of liquid;
D, constant equation (15) ($D = 3{\cdot}945 \times 10^3$ when ρ^* lb/in^3 and T_LK° used);
F_0, heat flux across nucleation site surface;
g, gravitational constant;
h, thickness of liquid film at the edge and base of the bubble;
i, integer indicating number of elapsed time steps each of Δt;
j, numerical identity for position of element points around the bubble surface;
k, thermal conductivity of liquid;
m, vapour mass;
δm_f, change in mass from liquid film over time Δt;
N, n, number of elements;
P_V, vapour pressure;
P_V^*, saturation pressure at temperature T_L;
P_L, liquid pressure;
$P_{L\infty}$, liquid pressure at the free surface;
P_{L0}, liquid pressure at nucleation site;
r, radial distance from centre of local bubble radius to point in liquid;
r_d', dried out radius at base of bubble;
r_d, new dried out radius at base of bubble after time Δt;
R_1, first principal radius } defined in
R_2, second principal radius } Fig. 1;
R, equivalent radius of curvature at a point on the bubble surface;
R_0, initial equivalent radius;
R_g, gas constant for the vapour;
S, length of sloping annular region occupied by the liquid film (see Fig. 3);
t, time from start of bubble growth;
Δt, time increment in the numerical procedure;
T_L, liquid temperature;
T^*, saturation temperature;
ΔT_L, change in liquid temperature;

$T_{L\infty}$, bulk liquid temperature;
T_W, temperature of the nucleation site solid wall;
U, bubble wall velocity;
U_n, bubble edge velocity;
V, bubble volume;
V_h, volume of nucleation site hole;
dV_f, volume of liquid evaporated from liquid film in time Δt;
x, horizontal coordinate from centre of nucleation site;
x_n, horizontal bubble radius at nucleation site surface;
y, vertical distance from nucleation site surface wall;
α, thermal diffusivity of liquid;
β, friction force at edge of bubble;
ζ, mass-transfer correction factor;
η, mass-transfer coefficient;
η_0, steady state mass-transfer coefficient;
$\bar{\eta}$, mean mass-transfer coefficient;
λ, latent heat of vaporization;
μ, liquid viscosity;
ρ^*, saturation density at temperature T;
ρ_V, vapour density;
ρ_L, liquid density;
σ, liquid surface tension;
ϕ, angle of propagation of an element point;
N_J, Jacob number $= \rho_L C_L (T_L - T^*)/\rho^* \lambda$.

Subscript
0, initial conditions.

1. INTRODUCTION

THE GROWTH and collapse of vapour bubbles in a liquid has been studied by many investigators, both experimentally and theoretically for many years. Rayleigh [1] in 1917 computed the pressure developed when a spherical cavity collapsed inwardly due to an external pressure field. Rayleigh's solution to the problem considered only the inertia of the liquid to be important and he neglected heat and mass transfer across the bubble interface. A complete solution to the problem requires that the continuity, momentum and energy equations for the liquid and vapour be solved simultaneously and coupled to mass and energy exchange across the interface.

In practice, to obtain any analytical solution, several simplifying assumptions are usually made. The most common one is that the bubble grows and collapses in a spherically symmetrical fashion. This assumption is made in the analyses of Forster and Zuber [2] and Plesset and Zwick [3]. The validity of the simplification has, however, been questioned by several experimentalists: both Hammitt *et al.* [4, 15] and Barclay *et al.* [5] have observed highly nonspherical collapse, usually in regions of large pressure gradients, while Johnson *et al.* [6] have observed a variety of bubble shapes during bubble growth.

In an attempt to shed some light on this complex problem we have developed an explicit finite difference marching technique, which obviates the necessity of assuming spherical growth. We assume, however, that the mass transfer component of the energy exchange across liquid vapour interface is the predominant mechanism and therefore heat transfer is ignored. The results obtained from this technique are compared to some experimental data published by Yessin and Jeffers [7] who studied the growth of bubbles from a nucleation site on a transiently heated metal strip.

2. THEORETICAL CONSIDERATIONS

The liquid–vapour interface is represented by a set of two dimensional axisymmetric elements as illustrated by Figs. 1a and 1b. We make the following assumptions:

(1) The liquid is incompressible.
(2) Energy exchange across the liquid–vapour interface is dominated by mass transfer.
(3) The surface topology of the bubble is characterised by a local radius of curvature which is the equivalent of the principal radii of curvature.
(4) The bubble interior is assumed to be uniform in both temperature and vapour density, obeying the equation of state.
(5) The liquid is static, having a one-dimensional

temperature and pressure distribution, hence the bubble is symmetrical about its vertical axis as in a static pool boiler.

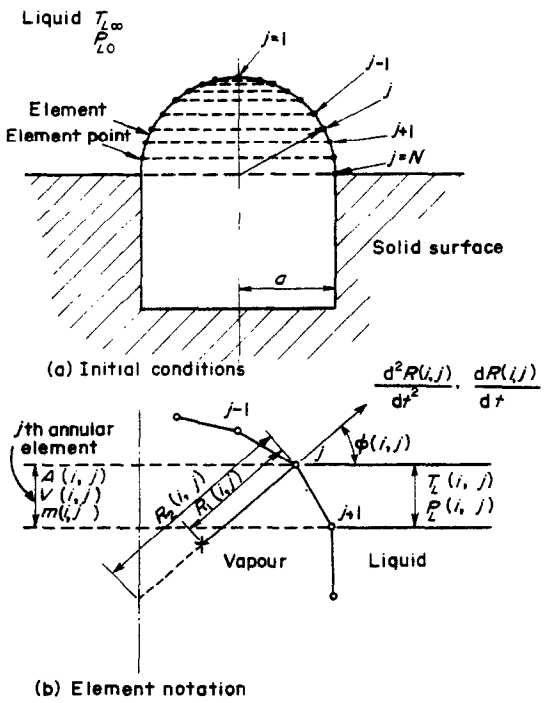

FIG. 1. Elemental representation of liquid–vapour interface.

(6) The initial shape of the bubble is hemispherical.

2.1 *Initial conditions*

Figure 1a shows the bubble surface equally divided by a number of element points. Initially the bubble is in static equilibrium with the surrounding liquid and the initial conditions are given by

$$P_V^*(T_{L\infty}) - P_{L0} = 2\sigma/R_0 \qquad (1)$$

from which the initial volume, vapour mass, density and surface area of each element can be calculated. We assume in equation (1) that there is no dissolved gas present in the bubble which is hemispherical and although these conditions are not strictly necessary they do simplify the initial setting of conditions prior to bubble growth. When the bubble grows, it may not always be spherical so its shape is characterised by the two principal radii of curvature R_1 and R_2. These are illustrated in Fig. 1b but both will vary with time and from point to point around the bubble surface.

It is convenient to define an equivalent radius R such that the surface tension pressure across any elemental surface is the same as it would be across an equivalent sphere of radius R; i.e. we define R by letting

$$2\sigma/R = \sigma\{1/R_1 + 1/R_2\}. \qquad (2)$$

This value of R can then be used in the modified Rayleigh equation as follows

$$\frac{P_V - P_L}{\rho_L} = R\frac{d^2R}{dt^2} + \frac{3}{2}\left(\frac{dR}{dt}\right)^2 + \left(2\sigma + 4\mu\frac{dR}{dt}\right)\frac{1}{R\rho_L} \qquad (3)$$

applying to all points on the bubble surface but slightly modified for the nth element point which moves along the solid nucleation site wall. Here a resistance force related to the magnitude of the periphery of the nth element and the surface roughness of the solid wall must be included in the brackets enclosing the surface tension and viscous forces. The extra term is $\beta/2\pi R(n)$ where β is the friction force per unit width of liquid displaced along the nucleation site surface (see for example J. J. Bikerman [8]).

The bubble can now be made to grow or collapse by any external disturbance. In this study we have imposed a sudden temperature disturbance by letting the temperature of the nucleation surface rise above the equilibrium liquid temperature at a rate equal to that measured by Yessin and Jeffers [7] during their experiments. At time t therefore, the temperature distribution in the liquid is given by

$$T_L(y, t) = T_{L\infty} + (T_W(t) - T_0)\,\mathrm{erfc}\left(\frac{y}{4\alpha t}\right), \quad (4)$$

which is a solution to the heat conduction equation given by Carslaw and Jaeger [9]. This temperature field will induce a corresponding change in the saturation vapour density and hence give rise to a potential to exchange mass across the liquid vapour interface. The incremental change of vapour mass will now increase the vapour pressure in the bubble which will grow according to the modified Rayleigh equation (3). It is important to note that although we assume the mass exchange across the bubble interface to be determined from local conditions, the driving pressure P_V is obtained by smearing out the incremental mass increase (or decrease) over the whole volume of the bubble.

2.2 *Explicit finite difference "marching" technique*

The numerical procedure is carried out in a step by step calculation of the bubble growth in the following way:

1. Set initial conditions with N number of points distributed uniformly around the bubble surface.
2. Calculate spatial temperature distribution after an incremental time step Δt.
3. Using the average temperature between the jth and $(j + 1)$ points calculate the mass exchanged across the elemental strip bounded by j and $j + 1$ in time interval Δt.
4. Sum the total mass transfer across the whole of the bubble interface including that transferred at the base of the bubble (δm_f), with the mass already in the bubble m so that the total mass at the ith time increment is,

$$m(i)_{(\mathrm{tot})} = \sum_{j=1}^{N} m(i, j) + \delta m_f. \quad (5)$$

Calculate new P_V due to mass transfer,

$$P'_V(i) = P_V(i - 1)\frac{m_{i(\mathrm{tot})}}{m_{(i-1)(\mathrm{tot})}}. \quad (6)$$

5. Calculate the equivalent radius of curvature at each element point from R_1 and R_2 such that

$$R(i, j) = 2\left\{\frac{R_1(i, j)\,R_2(i, j)}{R_1(i, j) + R_2(i, j)}\right\}. \quad (7)$$

where R_1 is given by the equation of the circle which passes through points $j - 1$, j and $j + 1$, and R_2 is the other principal radius which passes through the point j, the centre of R_1 and the bubble axis.

6. Movement of the element points over the next step Δt is obtained from the modified Rayleigh equation (3) in which $\mathrm{d}^2R(i, j)/\mathrm{d}t^2$ is calculated. The distance moved by an element point along R_2 therefore is

$$\Delta R(i, j) = \left[\frac{\mathrm{d}R(i - 1, j)}{\mathrm{d}t} + \frac{1}{2}\frac{\mathrm{d}^2R(i, j)}{\mathrm{d}t^2}\Delta t\right].\Delta t, \quad (8)$$

where $\mathrm{d}R(i - 1, j)/\mathrm{d}t$ is the velocity at time t and not at $t + \Delta t$, i being the time dependent coordinate in the element point array.

7. Sum the new elemental volume

$$V(i)_{(\mathrm{tot})} = \sum_{j=1}^{N} V(i, j) + Vh, \quad (9)$$

and modify $P'_V(i)$ to

$$P_V(i) = P'_V(i)\frac{V(i - 1)(\mathrm{tot})}{Vi(\mathrm{tot})}.$$

8. The new liquid–vapour boundary is given by the new element point positions, which are redistributed to maintain uniform element size.
9. Repeat the numerical procedure from step (2) increasing t by Δt each time round.

2.3 *Mass transfer*

Transfer of vapour mass across an elemental area is illustrated in Fig. 2 and can be described by kinetic theory which gives the evaporation rate as

$$\frac{dm}{dt} = \eta\left(\frac{R_g T_L}{2\pi}\right)^{\frac{1}{2}}(\rho^*(T_L) - \rho_V).A, \qquad (10)$$

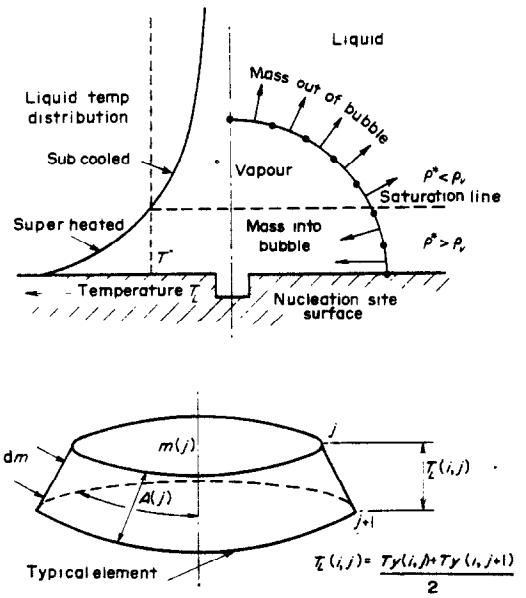

FIG. 2. Mass transfer across the liquid–vapour interface elements.

where η is an accommodation coefficient required to correct the theoretical result which assumes perfect evaporation (or condensation) at the designated bulk liquid temperature and vapour density conditions. The evaporation process is extremely complex and the energy exchange during evaporation results not only in the need for η which may vary, but also leads to a significant change in the temperature T_L at the interface, with the consequence that the rate of mass transfer is considerably reduced during evaporation, Hickman [10]. Although the behaviour of the accommodation coefficient in vapour bubble dynamics is still obscure, the dynamic behaviour of η postulated by Hickman in which the initial value of $\eta = 1{\cdot}0$ reduces to a much lower steady state value in a few milliseconds, would seem applicable. Whether or not the behaviour of η during evaporation is the same as that for condensation is also obscure; we assume here that it is. The magnitude of the steady state mass-transfer coefficient η_0 depends largely on the Jacob number N_J and for water it lies within the range 10^{-2}–5×10^{-2}, having its lowest value at highest superheat conditions (Theofanous *et al.* [12]). Alty [11] has found a value of $\eta_0 = 4 \times 10^{-2}$ for pure water evaporating into a vacuum.

Clearly the success of the theoretical approach described here is greatly influenced by the value of η used in equation (10), although it has been shown by Theofanous *et al.* [12] that a mean mass-transfer coefficient $\bar{\eta}$ can be successfully employed. This is particularly true for bubbles having rapid growth rate, and is the technique employed here.

Calculation of the local interfacial liquid temperature T_L and that of local vapour saturation density $\rho^*(T_L)$ present serious difficulties to the element method. This is because the precise nature of the interfacial thermal boundary profile must be obtained to facilitate the temperature drop calculation. Even in spherically symmetrical theoretical methods this problem is quite formidable and cannot be solved independently of the complete solution to the bubble growth, but it becomes even more intractable when the local liquid temperature and radius of curvature are not simply related to the vapour pressure within the bubble. For this reason we have been forced to employ the technique of using the local bulk liquid temperature condition ($T_{L\infty}$) and $\rho^*(T_{L\infty})$ in equation (10) and thus the accommodation coefficient η is now replaced by some factor ζ which will account for both the mean interfacial resistance and mean temperature drop.

For points around the liquid vapour interface therefore we use

$$\frac{dm}{dt} = \zeta\left(\frac{R_g T_{L\infty}}{2\pi}\right)^{\frac{1}{2}}(\rho^*(T_{L\infty}) - \rho_V).A. \qquad (11)$$

This simplification however can also be

justified for highly sub-cooled bubble growth since both rise and fall of the interfacial liquid temperature will occur due to the effects of evaporation and condensation energy exchange, and these will be compensatory to some degree. For the case of evaporation from a liquid film at the base of the bubble, however, the boundary conditions do permit a solution to the interfacial temperature drop problem.

2.4 *Evaporation from the base of the bubble*

Evaporation from a film of liquid at the base of a hemispherical or oblate bubble has been shown by Cooper and Lloyd [13] to be an important source of mass to the bubble. It is a simple matter to simulate this effect in the finite difference procedure, although the analytical solution in [13], based on the spherical bubble growth approximation in [3] may also be appropriate. We prefer to calculate the liquid film evaporation numerically. Figure 3 shows diagrammatically the film under the bubble and the dried out portion. From [13] the height of this microlayer h estimated from viscous boundary layer build up considerations is given by

$$h = C(\nu t)^{\frac{1}{2}}, \tag{12}$$

and the value of C has been estimated in [7] and [13] to be approximately 0·8. Assuming that the thickness of the thermal boundary layer is the mean height of the microlayer ($h/2$) we take the energy exchange across the liquid to vapour interface to be given by

$$\frac{dm_f}{dt} = \frac{2kA_b}{\lambda h}(T_L - T_W). \tag{13}$$

In addition we take, as before, the rate of evaporation (or condensation) to be given by

$$\frac{dm_f}{dt} = \zeta\left(\frac{R_g T_L}{2\pi}\right)^{\frac{1}{2}}\{\rho^*(T_L) - \rho_V\}A, \tag{14}$$

where in this case we use the value of T_L which satisfies equations (13) or (14) simultaneously.

By using an integrated form of the Clausius–Clapeyron equation to give

$$\rho^*(T_L) = \frac{D}{T_L}\exp(-B/T_L), \tag{15}$$

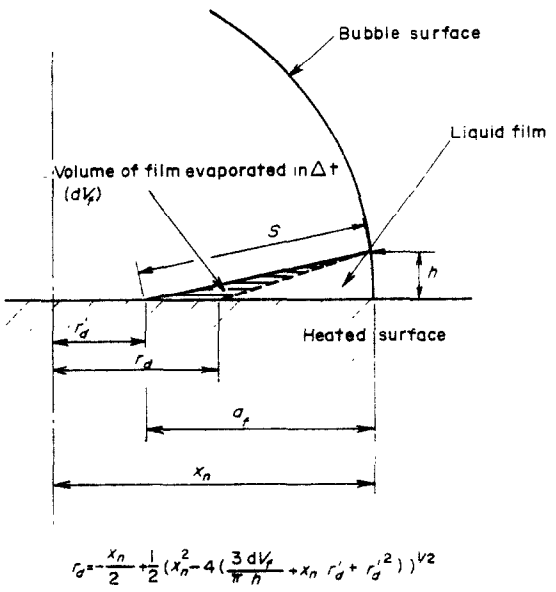

FIG. 3. Liquid film exporation at base of bubble.

then we may, from either (13) or (14) calculate the rate of mass transfer across the interface. This procedure is only valid if T_W and hence h and A_b are varying slowly with time compared to the rate at which the bubble grows. For the results presented in this paper the temperature of the wall changes by about 10 per cent while in same time the bubble volume increases many times. The use of this simplification therefore seems to be reasonable.

Again following Cooper and Lloyd [13] and taking the liquid microlayer to be in the form of frustrum of a cone of maximum height h, it is an easy matter to calculate the change in geometry of this frustrum by relating its change in volume to the amount of mass

evaporated by

$$\Delta V_f = \frac{\Delta m_f}{\rho_L},$$

where the geometry is as defined in Fig. 3.

3. LIQUID TEMPERATURE DISTRIBUTION

The one dimensional temperature distribution in a liquid surrounding a transiently heated surface, derived from the heat conduction equation is given by equation (4) from Carslaw and Jaeger [9]. When the heat flux F_0 rather than surface temperature T_W is known, an alternative solution also given in [9] is

$$\Delta T_L(y, t) = \frac{2F_0}{k}\left\{(\alpha t/\pi)^{\frac{1}{2}} \exp(-x^2/4\alpha t) - \frac{x}{2}\operatorname{erfc}(x/2(\alpha t)^{\frac{1}{2}})\right\}. \quad (16)$$

Since both of these forms are derived from heat conduction considerations alone, the calculated liquid temperature distribution becomes increasingly unrepresentative as t increases due to the increasing effect of thermal convection. Furthermore, in reality the temperature distribution in liquid above a nucleation site will also be affected by disturbances from adjacent active nucleation sites and by the bubble itself.

The problem of predicting temperature distributions during steady boiling is insoluble by analytical methods and no attempt to solve it numerically has been made in this study. However, Marcus and Dropkin [14] have attempted an empirical characterization of the steady boiling temperature profile dependent upon the heat flux at the solid surface, and this would appear to be applicable to finite difference bubble growth calculations for the steady boiling situation.

4. THE NUMERICAL PROCEDURES

4.1 *Initial conditions: number of elements*

As stated before, initial conditions depend largely upon the temperature of the nucleation site at the start of bubble growth. Thus the size of the site can be estimated from equation (1) when the site temperature at bubble inception is known. Although not strictly necessary, the assumption that the bubble is initially hemispherical in static equilibrium leads to a very simple initial condition. Element points which mark the annular element boundaries are uniformly distributed over the previously prescribed bubble shape or radius. Since we consider only the case of axial symmetry, the element points are distributed from $j = 1$ at the top of the bubble to $j = N$ at the edge of the hole as shown in Fig. 1a. The number of element points (N) is optional and although it may appear more accurate to have a large number of element points (i.e. small elements), there are certain difficulties which preclude this, namely, as with all numerical procedures we are limited by both computer accuracy and economy. If the elements are small the small difference in mass transfer across each element may be incorrectly computed due to computer round off errors. Differences in δm of the order 10^{-20} are possible in this type of procedure so it can be seen that even with double precision computation, truncation errors with small element calculations may be appreciable. The desirability of limiting computation time provides a further incentive for limiting the number of element points.

From our computations a suitable range for N would be between 10 and 20 depending upon the initial size of the bubble. However the problem associated with having too few elements (i.e. inaccurate representation of bubble topology) is greatly reduced by the introduction of a numerical surface movement of element points to prevent bunching or non-equal element spacing during computation. This is a simple mathematical technique to ensure that after each time step the independent movement of elements does not result in unequal spacing. It is achieved by rotating each element point about its local radius of curvature $R_1(i, j)$ in such a direction that the final distance between each element is equalised.

4.2 *Numerical stability*

As with many numerical solutions stability of the computations is critically affected by the mesh size, i.e. elemental size and magnitude of the time step. The element size effect has been discussed in 4.1 and now we consider the time step, again with the intention of obtaining optimum computational efficiency and numerical stability. The time step is calculated here as a function of element point acceleration, since equation (3) is most sensitive to the size of the time step. The criterion we have successfully used is

$$\left.\begin{aligned} &\text{for } \frac{d^2R}{dt^2} \leqslant 10^3, \quad \Delta t = 5 \times 10^{-8}\,\text{s} \\ &\text{for } \frac{d^2R}{dt^2} > 10^3, \quad \Delta t = \left(\frac{10^{-9}}{d^2R/dt^2}\right)^{\frac{1}{2}}\text{s} \end{aligned}\right\}$$

where R is in cm. The time step increases as acceleration d^2R/dt^2 decreases maintaining computational efficiency. This function produces a time step magnitude in the order of 10^{-9} s during maximum growth acceleration periods, usually in the initial stages of bubble growth, and was arrived at by running the computer program with several time step functions until stability was reached.

5. EXPERIMENTAL AND FINITE DIFFERENCE COMPARISON

Bubble growth from a nucleation site on a transiently heated stainless steel strip has been measured by Yessin and Jeffers [7]. Two of their results for liquid temperatures 90°C and 99°C at atmospheric pressure are considered here. The experimental conditions in both cases have been employed in the finite element computation and are given in Table 1, along with the appropriate ζ value which was selected to give the best agreement between the experimental and computed results. A set of ten elements represents the bubble surface in these numerical results and the liquid temperature distribution is given as a function of the measured temperature of the heated surface T_W by equation (4).

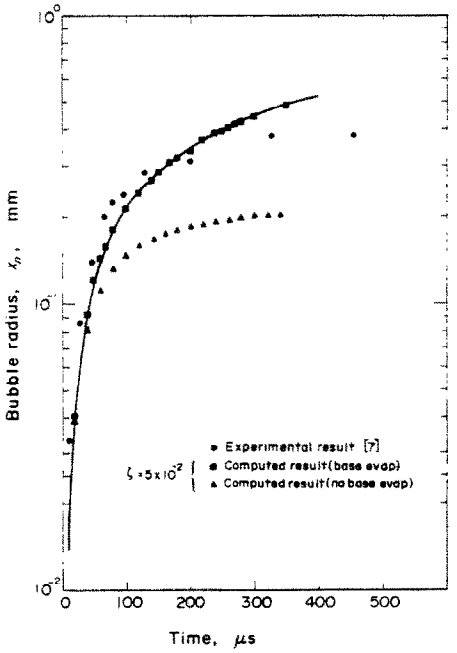

FIG. 4. Bubble growth $T_L = 90°C$.

5.1.1 *Bubble growth results.* Figure 4 shows the numerical bubble growth with and without mass

Table 1. Relevant experimental conditions [7]

T_L (°C)	Heated surface temperature at start of bubble growth (°C)	Nucleation site diameter (cm)	Wall temperature rise function ΔT (°C)	Mass transfer factor
90	116	$3{\cdot}32 \times 10^{-4}$	$6{\cdot}2 \times 10^{3}t$	$5{\cdot}0 \times 10^{-2}$
99	129	$1{\cdot}38 \times 10^{-4}$	$3{\cdot}67 \times 10^{4}t$	$3{\cdot}5 \times 10^{-2}$

transfer from the film of liquid beneath the bubble for $T_{L_\infty} = 90°C$ compared with that obtained experimentally. A similar comparison for $T_{L_\infty} = 99°C$ is shown in Fig. 5. Agreement between the experimental and numerical results with film evaporation is good over the range of bubble growths compared, although this is in results with time. Good agreement in the bubble growth comparison gives a degree of confidence in the many other numerical results such as volumetric and vapour mass growth rates, dry out radius and liquid film temperature, bubble pressure and acoustic emission in the liquid above the bubble. Instantaneous accelera-

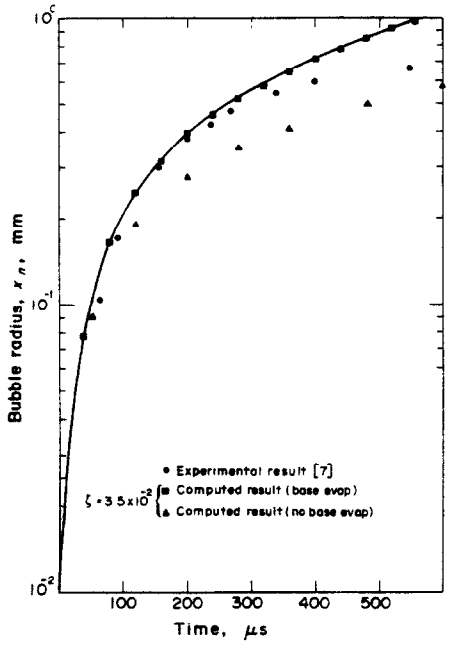

FIG. 5. Bubble growth $T_L = 99°C$.

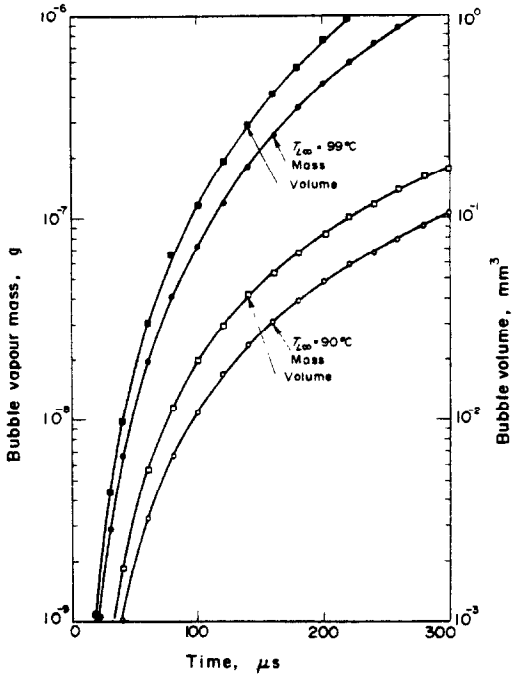

FIG. 6. Computed bubble volume and vapour mass with time.

largely due to the arbitrary selection of a value for ζ in equation (11). Interference from other nucleating bubbles when $t > 0.5 \times 10^{-3}$ seconds from the start of bubble growth was a limitation in the experimental measurement, but according to photographic evidence in [7] interference from other bubbles may well have started earlier. In the numerical result, we must recognise that the activity of other sites and the increasing effect of thermal convection sets a similar time limit for computational accuracy and this accounts for the increasing discrepancy tion, velocity and local radius of curvature for the bubble are also known but are more difficult to summarize here. Increase in vapour mass and bubble volume with time for $T_L = 90°C$ and 99°C are plotted in Fig. 6. The ratio of the dryout radius and bubble edge radius (r'_d/x_n) is plotted in Fig. 7 for the two bulk liquid temperatures, and the computed results for the drop in liquid film temperature are shown in Fig. 8. Variation in computed bubble vapour pressure P_V with time, for the two liquid temperatures is shown in Fig. 9 normalized to the liquid surface

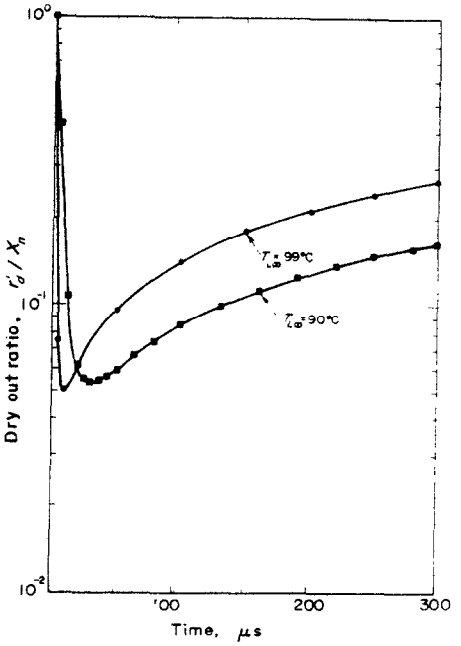

FIG. 7. Ratio of dried out radius to bubble edge radius with time.

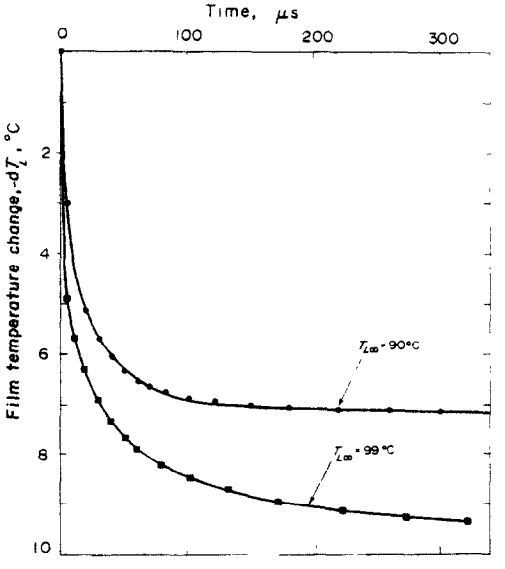

FIG. 8. Computed change in liquid film temperature with time.

pressure. The bubble is seen to grow in a spherical manner in the computed results of Fig. 10a for $T_{L\infty} = 90°C$ and 10b for $T_{L\infty} = 99°C$. The bubble shape on collapse however is more complicated and worthy of special explanation.

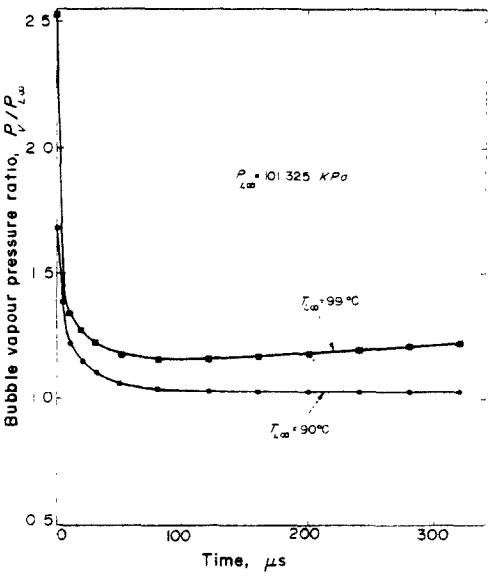

FIG. 9. Computed variation in bubble vapour pressure with time

5.1.2 *Bubble shape during collapse.* To study the shape of the bubble during total collapse a computation was carried out with the same condition as for the $T_{L\infty} = 90°C$ but with no base evaporation (see Fig. 4) and with the modification that after $2{\cdot}0 \times 10^{-4}$ s growth, the liquid temperature became equal to the bulk conditions $T_{L\infty} = 90°C$ everywhere. Thus the event of convection cooling which would precipitate collapse in the real case was simulated in a crude way. The resulting bubble shape during collapse is extremely interesting. Figure 11 shows that the shape of the bubble becomes highly non-spherical near to the completion of the collapse phase, and in the centre region the downward liquid velocity becomes very high.

The unusual shape of the bubble does however lead to an increasingly inaccurate numerical result due to the fact that the radius $R(1)$ at the centre of the bubble is over estimated. The error involved therefore has the effect of under estimating the collapse velocity in that region. This result is in agreement with Hammitt [4, 15] and Barclay, Ledwidge and Cornfield [5] who have studied the damage caused by collapsing vapour bubbles and observed highly non-spherical bubble shapes. Hammitt concludes that an enlarged pit forms at the nucleation site due to the impulse of a high velocity liquid jet produced during this type of bubble collapse: we see the formation of this jet in Fig. 11. The acoustic pressure in the liquid above the bubble is also greatly affected by the central concavity during collapse and is found numerically to display totally different characteristics to the noise during bubble growth.

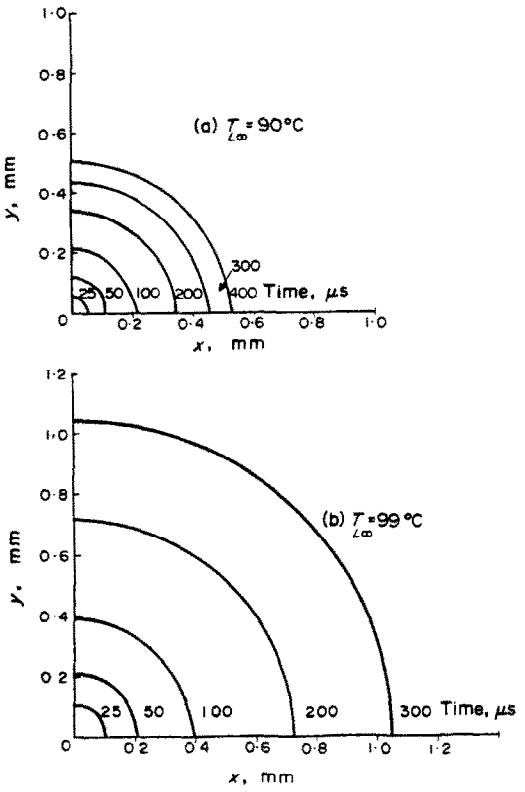

FIG. 10. Bubble shape during growth.

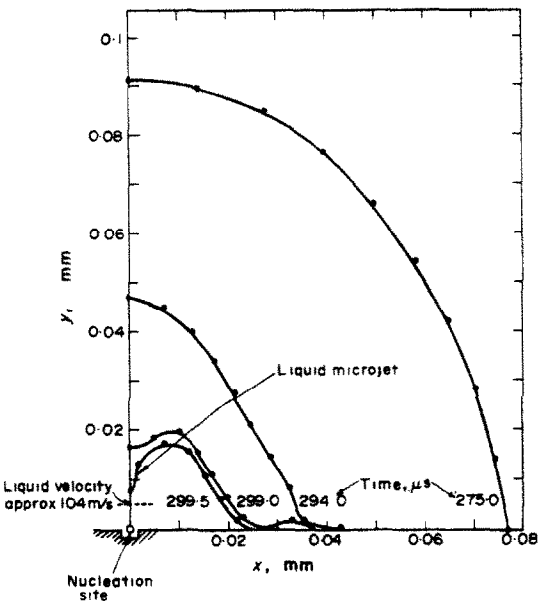

FIG. 11. Computed bubble shape during collapse, $T_{L\infty}$ = 90°C (no base evaporation).

5.2 *Liquid pressure above the bubble*

The water pressure at approximately 10 mm directly above the nucleation site was calculated during the bubble growth computation, and this result provides information on how the bubble noise relates to this type of growth or collapse. Figure 12 shows this result for the 90°C and 99°C bulk liquid temperatures, and although the pressure is plotted on a logarithmic scale the large characteristic difference in noise due to different subcooling conditions can be seen easily.

The liquid acoustic pressure derived from the

Rayleigh equation (3) is given by

$$\Delta P_L = \frac{R_{(j=1)}}{r}\left[\Delta P_V + \frac{1}{2}\frac{\rho_L U^2(j=1)}{g} \times \left\{1 - \left(\frac{R_{(j=1)}}{r}\right)^3\right\}\right] \quad (17)$$

where $\Delta P_V = P_V - P_L - 2\sigma/R_{(j=1)}$. During collapse it is possible for any part of the bubble surface to become concave to the liquid with the noise characteristic of this type of collapse. Until the start of collapse the acoustic pressure is characteristically the same as that shown for $T_{L\infty} = 90°C$ in Fig. 12. In the Fig. 13 result, however an arbitrary step change in liquid temperature brings about collapse after 200 μs and although the overall result may be some-

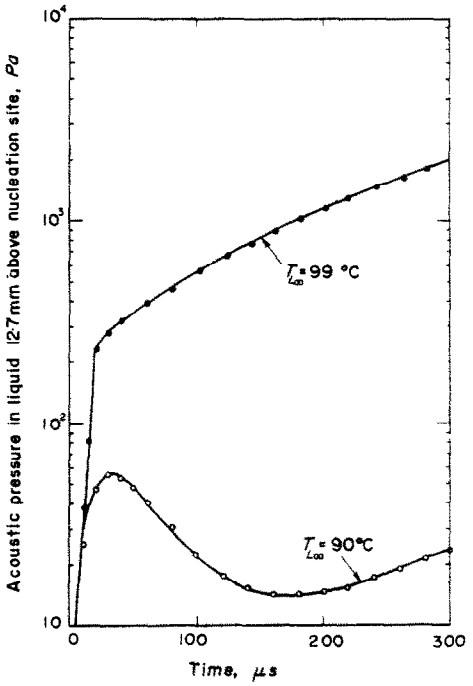

FIG. 12. Computed bubble growth noise directly above the nucleation site.

result that the local acoustic emission will be greatly affected. As the surface becomes concave $R \to \infty$ and $R/r \to 1{\cdot}0$, therefore $\Delta P_L \to \Delta P_V$, and thus the upper limit of such a peak would be ΔP_V and not infinity, as would occur during the very last stages of bubble collapse according to Rayleigh's analysis. The collapsing bubble shape does indeed show concavity in its later stages (Fig. 11) and by plotting the liquid pressure above the bubble, as in Fig. 13 we see the bubble

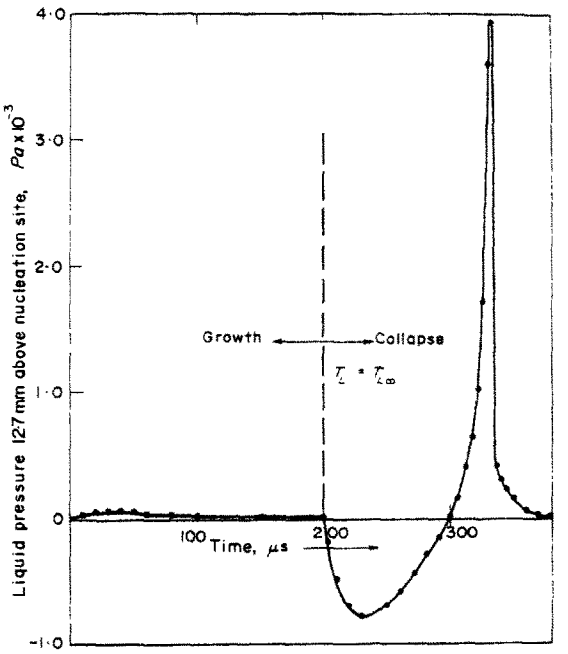

FIG. 13. Bubble noise computed for growth and collapse stages $T_\infty = 90°C$.

what artificial, it does serve to illustrate the different type of noise signal during the two different phases of bubble life. It follows that in the case when the bubble wall oscillates from a concave to a convex shape one might expect to see a series of bubble noise peaks reaching a maximum pressure level of

$$\Delta P_L = P_V - P_L - 2\sigma/R.$$

6. CONCLUSIONS

Good agreement between experimental and computed bubble growth in water bulk temperatures of 90°C and 99°C at atmospheric pressure.

has shown that the finite difference model can successfully represent vapour bubble dynamics under the prescribed experimental conditions.

The technique of matching one experimentally determined parameter by a corresponding numerical result has been shown to be a useful way of determining theoretically, through the finite difference method, a range of other parameters for which experimental measurement is too difficult. A further example of this technique has already been carried out (Guy and Ledwidge [16]), where the noise measured during bubble growth was compared with that computed numerically. The importance of employing the correct variable mass-transfer coefficient or a mean value which accurately represents a mean of the initially transient coefficient is emphasized. As yet there is no way of theoretically determining a value for $\eta(t)$ or $\bar{\eta}$ but η may be found by trial and error. We note with interest the fact that in our numerical results the most appropriate values of ζ used in the mass transfer equation (11) were $3{\cdot}5 \times 10^{-2}$ for $T_L = 99°C$ and 5×10^{-2} for $T_{L_\infty} = 90°C$, which compares with Theofanous *et al.* [12] who found in their numerical results that the most appropriate value for the mean mass-transfer accommodation coefficient lay between 10^{-2} and 5×10^{-2}. As pointed out earlier $\bar{\eta}$ is different to the factor ζ which is designed to account for interfacial liquid temperature changes as well as embracing the accommodation coefficient. It can be argued therefore that in sub-cooled bubble growth, the increase in liquid interfacial temperature on the condensation surface balances to some extent the decrease in temperature at the evaporation surface.

The numerical computations also show that evaporation from the liquid film at the base of the bubble cannot be neglected particularly when bubble growth becomes well established. Indeed, for the highly sub-cooled bubble growth after about 100 μs growth time, the continued growth of the bubble relies entirely upon evaporation from the base of the bubble. It is anticipated that future development of this method of vapour bubble analysis will allow accurate simulation of temperature fluctuations at the heated surface T_W, thus providing greater understanding of several heat transfer problems at present under study, e.g. burnout on nuclear fuel elements.

ACKNOWLEDGEMENTS

The authors would like to thank Mr. P. J. Ryan for his assistance in writing the computer program

REFERENCES

1. Lord Rayleigh, *Phil. Mag.* **34**, 94 (1917).
2. H. Forster and N. J. Zuber, *Appl. Phys.* **25** (4), 474–478 (1954).
3. M. Plesset and S. Zwick, *J. Appl. Phys.* **25** (4) 493–500 (x954).
4. F. G. Hammit, *Proc. Instn Mech. Engrs* **183**, 1, (1), 31–50 (1968–69).
5. F. J. Barclay, T. J. Ledwidge and G. C. Cornfield, *Proc. Instn Mech. Engrs* **183**, 1 (2), 43 (1968–69).
6. M. A. Johnson, P. De La Javier, and R. B. Mesler, *A. I. Ch. E. Jl* **12**, 344–348 (1966).
7. A. O. Yessin and D. E. Jeffers, *J. Br. Nucl. Energy Soc.* **8** (4), (1969).
8. J. J. Bikerman, *Physical Surfaces*. Academic Press, London (1970).
9. H. S. Carslaw and J. C. Jaeger, *Conduction of Heat in Solids*, p. 23. Oxford University Press (1959).
10. K. Hickman, 1st Int. Symp. on Water Desalination, pp. 180–217, SWD/27 (1965).
11. T. Alty, *Phil. Mag.* **15**, 82–102 (1933).
12. T. Theofanous, L. Baisi, H. Isbin and H. Fouske, *Chem. Engng Sci.* **24** (5), 885–899 (1969).
13. M. G. Cooper and A. J. P. Lloyd, *Int. J. Heat Mass Transfer* **12**, 895–933 (1969).
14. B. D. Marcus and D. Dropkin, *J. Heat Transfer*, 333–341 (1965).
15. C. L. Kling and F. G. Hammitt, *J. Basic Engng* 825–833 (Dec. 1972).
16. T. B. Guy and T. J. Ledwidge, Proc. 4th Australasian Conference on Hydraulics and Fluid Mech., Monash University, Melbourne, pp. 345–351 (1971).

APPROCHE NUMERIQUE DE LA DYNAMIQUE D'UNE BULLE DE VAPEUR NON SPHERIQUE

Résumé—Une analyse explicite aux différences finies est appliquée à la croissance et à la disparition d'une bulle de vapeur dans de l'eau sous-refroidie. On suppose que seul est important le transfert de masse à travers l'interface liquide–vapeur et que le transfert thermique peut être négligé. Les résultats de ce calcul comparés aux données de l'expérience, sont en bon accord pour des sous-refroidissements de 1°C et 10°C.

Pour ces conditions expérimentales les analyses montrent que les bulles croissent de façon à peu près sphériques mais dégénèrent de façon très éloignée de la forme sphérique.

EINE NUMERISCHE NÄHERUNG ZUR NICHT-SPHÄRISCHEN BLASENDYNAMIK

Zusammenfassung—Es wurde ein explizites Differenzenverfahren angewandt zur Berechnung von Wachstum und Kollaps einer Dampfblase in unterkühltem Wasser. Dabei wurde angenommen, dass nur der Massentransport über die Flüssigkeits-Dampf-Grenze bedeutsam ist, während der Wärmeübergang vernachlässigt werden kann. Die Ergebnisse dieser rechnerischen Untersuchung werden mit experimentellen Ergebnissen aus der Literatur verglichen und zeigen gute Übereinstimmung bei 1 K und 10 K Unterkühlung.

Für die experimentellen Bedingungen zeigt die Untersuchung, dass die Blase in angenähert kugeliger Form wächst, aber in stark asphärischer Gestalt zusammenbricht.

ЧИСЛЕННЫЙ АНАЛИЗ ДИНАМИКИ НЕСФЕРИЧЕСКИХ ПУЗЫРЕЙ ПАРА

Аннотация—Явная конечно-разностная схема используется для анализа роста и слияния пузырей пара в недогретой жидкости (воде). Учитывается только поперечный перенос массы через поверхность раздела «жидкость-пар», а теплообменом пренебрегают. Результаты этого численного анализа сравниваются с экспериментальными данными, опубликованными в литературе, причем сравнение показало хорошее совпадение при недогреве от 1°C до 10°C.

Для рассматриваемых экснериментальных условий анализ показывает, что рост пузырей можно приближенно представить с помощью сферической модели, а слияние пузырей в высшей степени несферично.